A parallel two-way split-step wavelet method for the tropospheric propagation

Thomas Bonnafont
Lab-STICC, UMR CNRS 6285
ENSTA Bretagne
Brest, France
thomas.bonnafont@ensta-bretagne.fr

Corentin Carré
Lab-STICC, UMR CNRS 6285
ENSTA Bretagne
Brest, France
corentin.carre@ensta-bretagne.fr

Ali Khenchaf
Lab-STICC, UMR CNRS 6285
ENSTA Bretagne
Brest, France
ali.khenchaf@ensta-bretagne.fr

***Abstract*—Modeling the atmospheric long-range propagation is an important step in the development of observation, satellite, or communication systems. This paper presents a parallelized version of the two-way split-step wavelet method, designed to enhance computational efficiency. Numerical experiments in the UHF band are provided to highlight the benefits of the proposed method. In the studied cases, we observe a 25%-60% gain in terms of computation time, depending on the terrain taken into account. The proposed approach is also leveraged to generate a dataset for training a machine-learning model based on the U-Net architecture.**

***Index Terms*—long-range propagation, split-step method, wavelet, parallel programming, machine learning**

I. Introduction

Accurate modeling of tropospheric long-range propagation is essential for applications such as predicting system coverage, optimizing antenna placement (e.g., for 5G networks), and assessing the impact of structures on system performance. In this context, one should consider the effect of the relief, refraction, and ground composition to obtain an accurate field prediction.

A widely used model in this context is the parabolic wave equation (PWE) [1]–[3]. Indeed, this latter omits the backward propagation allowing wide steps in the propagation direction. The split-step Fourier (SSF) [1], [3] or the split-step wavelet (SSW) [4]–[6] methods can be used to efficiently solve the PWE while accounting for the relief, the refraction, and the ground composition.

Both methods rely on computing the field iteratively with two steps at each iteration. The field is first propagated in a free-space layer either in the Fourier domain, for SSF [3], or in the wavelet domain, for SSW [4], [5]. Then, a phase screen [1], [3] is applied in the spatial domain to take into account the refraction. The effects of the relief and the ground composition are also introduced in the spatial domain [2], [3].

Nonetheless, in this case, the reflections, when reaching obstacles, are omitted. To overcome this problem, a two-way PWE solved with SSF has been proposed in [7], [8]. This latter has been efficiently introduced in SSW [9], using the advantage of compression. In this case, when the field reaches an obstacle both the backward and forward waves are propagated using either SSF or SSW, leading to a fast increase of the computation time.

The objective of this article is twofold. First, a parallel version of two-way SSW is proposed to overcome the computation time burden. Indeed, our objective is then to hybridize this method with a Method of Moments as in [10], or to use it to make reliable artificial data for machine learning models, see [11], [12] for examples. In both cases, computation time must be as low as possible. Second, the parallel two-way SSW method is used as an input to train a machine-learning model. The latter is based on a modified U-Net architecture [12]–[14].

The remainder of this article is structured as follows. Section II focuses on the parallel implementation of the two-way SSW method. In Section III, some numerical experiments are performed in the UHF-band in order to highlight the advantages of the proposed method. Section IV introduces a machine learning model for predicting path loss over rural terrain using the proposed two-way SSW method as the underlying model. Finally, Section V concludes the paper and gives perspective for future works.

II. A parallel two-way split-step wavelet method

A. The two-way PWE model

Throughout the paper, an $\exp(j\omega t)$ time dependence is assumed, with $\omega = 2\pi f$ the angular frequency and f the frequency. We also denote by n the refractive index and by k_0 the wave number.

The propagation is computed in a 2D domain, where the usual Cartesian coordinate system (x, z) is used, with x the propagation axis and z the altitude. We assume that the field, denoted by Ψ, is known at $x = 0$. The propagation is computed until $x_{\max}$ above the ground, i.e., $z \geq 0$. Therefore, the objective is to obtain Ψ in $[0, x_{\max}] \times [0, z_{\max}]$.

Under these conditions, the field can be decomposed into its transverse magnetic (TM) and transverse electric (TE) components. Since for both computations remain the same, here we study the TE case. Indeed, they are both solutions of a scalar Helmholtz equation.

To obtain the two-way parabolic equation (PWE), the field Ψ is decomposed into two components as

$$\Psi(x,z) = \exp(jk_0x)u_{\mathrm{F}}(x,z) + \exp(-jk_0x)u_{\mathrm{B}}(x,z), \quad (1)$$

with u_{F} and u_{B}, the forward and backward reduced fields [7], respectively. The two are solutions of

$$\begin{aligned} \frac{\partial u_{\mathrm{F}}}{\partial x} &= -jk_0\left(\sqrt{\tfrac{1}{k_0^2}\tfrac{\partial^2}{\partial z^2}+1}-1\right)u_{\mathrm{F}} - jk_0(n-1)u_{\mathrm{F}}, \\ \frac{\partial u_{\mathrm{B}}}{\partial x} &= jk_0\left(\sqrt{\tfrac{1}{k_0^2}\tfrac{\partial^2}{\partial z^2}+1}-1\right)u_{\mathrm{B}} + jk_0(n-1)u_{\mathrm{B}}. \end{aligned} \quad (2)$$

The latter correspond to the forward and backward propagations, respectively, and are different only by the sign of k_0. In

the usual PWE model, only the first equation is used, since only the forward propagation is accounted for, whereas here the backward propagation is used when we reach an obstacle.

In the following sections, we introduce a parallel method to efficiently solve these two equations.

B. An overview of one-way SSW

In this section, the one-way version of SSW [5] is explained, since it is used as the core of the parallel two-way SSW method.

First, let us introduce the discretization and the notations we use. The domain is discretized along the z-axis with a step size Δz and along the x-axis with a step size Δx. With $p_z \in [0, N_z]$, we have $z_{p_z} = p_z \Delta z$, where $N_z = z_{\max}/\Delta z$. The field at a position x is denoted by $u_x[\cdot]$.

Second, the SSW algorithm is quickly reminded, for more details see [4], [5]. This latter computes iteratively the field by going back and forth in the wavelet and spatial domains. One step of propagation from x to $x + \Delta x$ is performed as follows:

1) The sparse vector of wavelet coefficients U_x, associated with the field u_x is obtained as
$$U_x = \mathbf{C}_{V_s} \mathbf{W} u_x,$$
where $\mathbf{W}$ corresponds to the fast wavelet transform (FWT), and $\mathbf{C}_{V_s}$ to compression with hard threshold V_s.
2) The field is propagation, assuming a free-space layer, in the wavelet domain as
$$U_{x+\Delta x} = \mathbf{P}_{V_p} U_x,$$
where $\mathbf{P}_{V_p}$ corresponds to a sparse wavelet-to-wavelet propagator [5]. The latter contains the compressed (threshold V_p) wavelet coefficient associated with the propagation of each wavelet of the basis.
3) We come back in the spatial domain, using an inverse FWT, to take into account the effect of the refraction, and the relief
$$u_{x+\Delta x} = \mathbf{R}\mathbf{L}\mathbf{W}^{-1} U_{x+\Delta x},$$
with $\mathbf{W}^{-1}$ the inverse FWT, $\mathbf{L}$ the phase-screen operator [1], [3] to take into account the effect of the atmosphere, and $\mathbf{R}$ that accounts for the relief (staircase model [3]).

Finally, the effect of the ground is efficiently accounted for using the local image method [4]. This latter allows us to model the ground through the Fresnel coefficient with a reduced number of points.

C. The parallel two-way SSW method

Now that the one-way SSW method has been reminded, we can focus on its recursive two-way counterpart.

As the equations for u_{F} and u_{B} are the same within the sign before k_0, and the fact that we are propagating the first toward $+x$ and the second toward $-x$, both propagators are the same [7]. Therefore, the idea is to use recursively the one-way SSW to solve back and forth the forward and backward propagation equations when reaching obstacles [7]–[9]. A schematic representation of the method is pictured in Fig. 1.

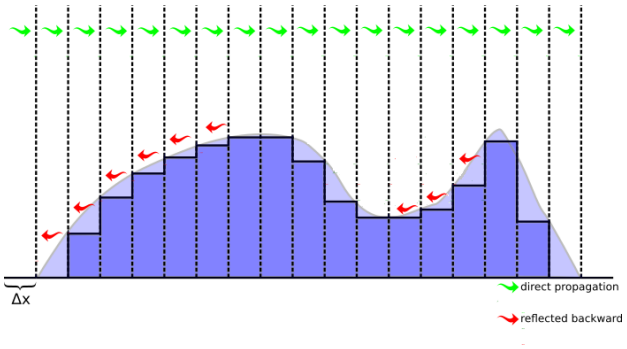

Fig. 1: Example of a two-way propagation.

First, the field is propagated forward, pictured in green arrows in Fig. 1, until an obstacle is encountered at position x_o. Here, we compute the initial field for the backward propagation using

$$\Psi(x_o) = t \exp(jk_0 x_o) u_{\mathrm{F}}(x_o) = \exp(jk_0 x_o) u_{\mathrm{F}}(x_o) + \exp(-jk_0 x_o) u_{\mathrm{B}}(x_o), \quad (3)$$

where t is the transmission coefficient. This condition aligns with the transverse field condition due to the utilization of a staircase model. For example, in the case of a PEC, we have $\Psi(x_o) = 0$. Then the backward field, pictured with red arrows in Fig. 1, is computed from x_o until 0 using $u_{\mathrm{B}}(x_o)$ as the initial field. These steps are repeated at each encountered obstacle.

It is important to note that the computational burden of this method increases rapidly with the number of staircases needed to represent the relief, since at each one a backward propagation needs to be computed. To address this, we propose a parallel version of the method in this paper, that drastically reduces the computation time by leveraging multiple cores for handling the multiple reflected propagations.

The primary challenge lies in establishing the connection between forward and backward propagations. Specifically, at each relief point, the reflection is computed from the incident forward field, as outlined in Eq. (3). For now, let's consider a scenario where only the backward propagation is considered. This approach can be extended for multiple reflections, requiring numerous cores.

In this case, the idea is to obtain the relief map in the propagation axis, i.e. where the reflections need to be computed. This corresponds to the position of the rising steps here. The forward propagation is executed until each ascending step, where it is then split into the forward and backward propagation, each assigned to different cores. The backward part is propagated towards 0, while the forward propagation continues until the next ascending step. Finally, all the backward propagations are combined with the forward propagation to yield the total field. For instance, in Fig. 1, one core would handle the forward propagation (green arrows), while each backward propagation (red arrows) would be assigned to different cores.

III. Numerical tests

In this part, some numerical tests are performed to highlight the advantages of the proposed parallel two-way SSW method. Those tests are carried out at $f = 300$ MHz in the

UHF band (more precisely in the C-band). Besides, all the computations are performed using a desktop computer with a 10-core i5 processor.

A. A canonical test

First, the method has been tested on a simple canonical case, where some knife-edge reliefs are accounted for. Indeed, we consider two knife-edge and one triangular obstacles located at 10 km, 16 km, and 50 km of respective heights 100 m, 300 m and 200 m.

The propagation is computed for $x \in [0, 100]$ km and $z \in [0, 1024]$ m. The antenna is modeled by a complex source point (CSP) [15] placed at $x_s = -50$ m and $z_s = 120$ m, with a width of 5 m. The ground is assumed to be a PEC, and the refractive index to be constant $n = 1$. For the thresholds in SSW, we set them to have an error of at most -30 dB with SSF at the last iteration, using the theoretical formula given in [16].

In Fig. 2, we plot the field obtained with the parallel two-way SSW in (a), and the normalized absolute difference with the non-parallel version [9] in (b).

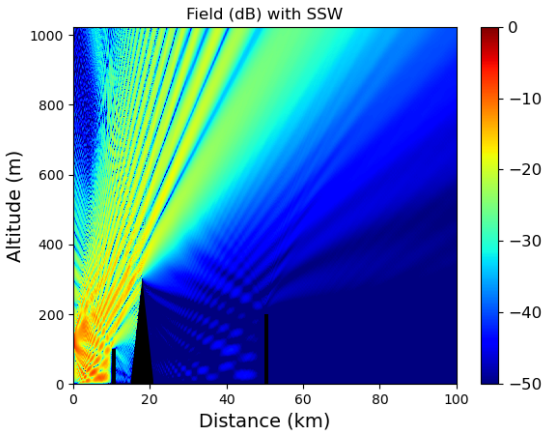

(a) Field computed (dB) with parallel two-way SSW.

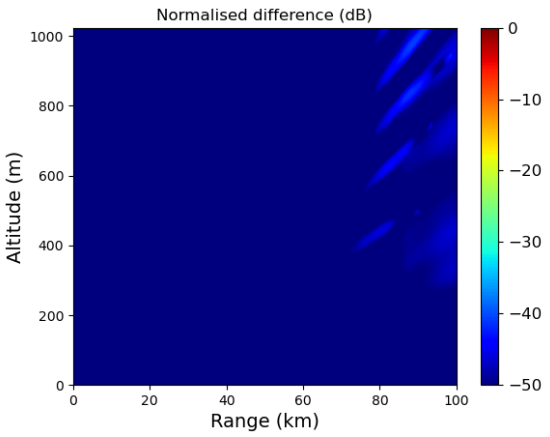

(b) Normalized difference in (dB).

Fig. 2: Results for the canonical test.

As expected, the same results are obtained with the parallel and non-parallel methods, see Fig. 2 (b). Indeed, the reflections at each obstacle are visible. Besides, the computation for the parallel version is 16 s, while for the usual method it is 24 s. In this context, we thus observe a gain of 33% in terms of computation time compared to using only one core.

B. Application: propagation from Toulouse to Montauban

Second, we study a scenario closer to reality. Indeed, we want to obtain the coverage of the antenna placed in Toulouse (France), in one direction. This could be useful to optimize its location, for example for the Toulouse airport radar antenna.

Therefore, we aim to compute the electromagnetic propagation from Toulouse to Montauban, two cities distant from 50 km. The terrain between both is obtained through the IGN data [17]. The parameters remain the same as the previous test, except that a tropospheric duct is accounted for. The latter is modeled using a tri-linear refractive profile [18] with parameters : $M_0 = 330$ M-units, $c_1 = 0.118$ M-units/m and $c_2 = -0.5$ M-units/m for the gradients, and $z_b = 300$ m and $z_t = 250$ m.

As before, in Fig. 3 (a) we plot the field computed with the proposed parallel two-way SSW. The normalized difference with the non-parallel method is presented in (b).

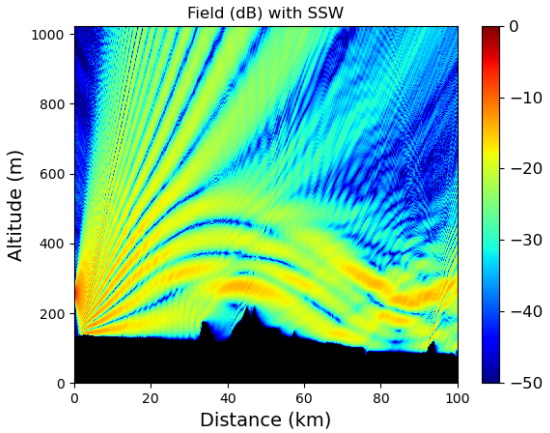

(a) Field computed (dB) with parallel two-way SSW.

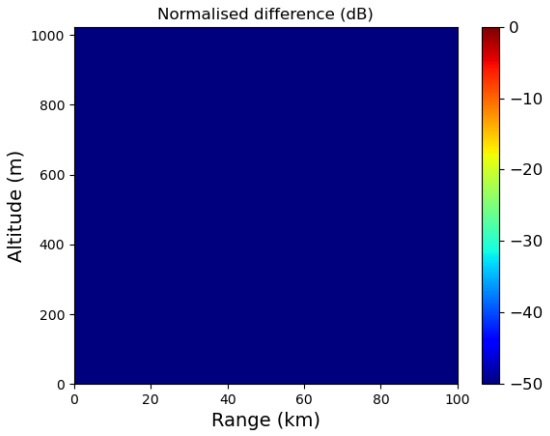

(b) Normalized difference in (dB).

Fig. 3: Predicted coverage from Toulouse to Montauban.

Here, the propagation is computed in 174 s with the parallel code, while it took 464 s with the non-parallel version. This corresponds to an acceleration of more than 60%. Indeed, compared to the canonical test, the model of the relief is more complicated leading to more reflections to account for.

Besides, as expected, the result with both methods is the same, see Fig. 3 (b).

Therefore, the parallel two-way SSW allows a drastic reduction of the computation time, in particular when the terrain considered becomes closer to reality.

IV. A DEEP TWO-WAY SSW METHOD

In this part, we present an application where the acceleration provided by the parallelization is useful: implementing a deep two-way SSW method. The objective here is to predict the path loss at the height of the antenna given an input terrain, as in [12].

A. The architecture

The idea of the machine learning model is to approximate the function f, by a function $\hat{f}_\theta$, which maps the input physical phenomena (Φ) – such as terrain data, the refraction, or ground composition– to a path loss prediction ($\hat{y}$). In this definition, θ corresponds to network's weight, and $|\theta|$ denotes the dimension of the network parameters.

In this context, the input Φ considered is the 1D vector of size N_x containing the terrain data, i.e. the altitude at each step Δx. Therefore, we have $\Phi \in \mathbb{R}^{N_x}$. The objective here is to map this latter to a path loss prediction $\hat{y}$ at the transmitter altitude, thus $\hat{y} \in \mathbb{R}^{N_x}$, through the function $\hat{f}_\theta$.

In this work, we use supervised machine learning. Indeed, we use data computed with the parallel two-way SSW method to train the network. Thus, the function $f : \Phi \mapsto y$ corresponds here to the proposed parallel SSW method.

For this study, supervised machine learning is employed. The network is trained using data generated through the parallel two-way SSW method, thus corresponding to $f : \Phi \mapsto y$.

Since it has shown good results in related areas [12], [14], a modified U-Net architecture is used here.While U-Net was originally designed for image processing [13], we adapt it by using 1D convolutions in place of the 2D convolutions.

This network consists of two main parts: the descending part that allows the feature detection, and the ascending part, in charge of the regression[1].

In more detail, the first part seeks to extract useful information from the input vector – the terrain profile, in this case. To do so undergoes 5 levels of convolution, batch normalization, ReLU activation windows, and subsampling to condense the information into a latent space containing only the essential terrain features. To limit $|\theta|$ the convolution kernels are of size 5, and they are widened with a dilation rate as in [14]. This latter is amplified throughout the feature detection part to capture details further away for lower scales without increasing the number of parameters θ.

Moving to the second part, the network focuses on constructing the path loss prediction from the features obtained in the initial stage. The second stage also consists of 5 levels, where we go from the lowest scale – or details about the terrain – to the largest one through transpose convolutions, convolutions, batch normalization, ReLU activation, and upsampling using skipped connections. All the convolution kernels are of size 2, except the last which is of size 1 to retrieve $\hat{y} \in \mathbb{R}^{N_x}$.

[1]Note that this architecture reminds of SSW where $\mathbf{C}_{V_s}\mathbf{W}$ could be seen as the descending part and $\mathbf{W}^{-1}\mathbf{P}_{V_p}$ as the ascending part

B. Training of the network

In order to train the network, we first need to define an appropriate objective function, referred to as the loss function. This metric quantifies the proximity of predicted data $\hat{y}$ to the actual observations y. For this regression problem, we opt for the widely-used mean square error (MSE) [12]. This leads to the following empirical risk to be minimized:

$$\inf_{\theta \in \mathbb{R}^{|\theta|}} \mathbb{E}_{\phi \sim \mathcal{L}_\phi} \left\{ \|f(\phi) - \hat{f}_\theta(\phi)\|_2^2 \right\}, \tag{4}$$

where $\mathcal{L}_\phi$ corresponds to the distribution of the samples ϕ used to train the network.

Ideally, we want the latter to uniformly cover the manifold of the physical phenomena while remaining memory and computationally efficient. In this case, since a staircase model is employed to describe the terrain, the dataset consists of obstacles of triangular and rectangular shapes. To ensure a well-distributed representation of the associated manifold, we employ a Latin Hypercube Sampling (LHS) strategy. This creates triangle and/or rectangle obstacles of different sizes at varying positions. In more detail, the dataset consists of 1000 samples for terrain containing between 2 to 5 obstacles, leading to 4000 samples in total. The latter is equidistributed concerning the number of obstacles. We choose to focus here on rural environments, with relief altitudes ranging from 0 to 65 m. Finally, we consider the transmitter at $z_s = 70$ m and a domain of size $x \in [0, 80]$ km with $\Delta x = 50$ m, leading to $N_x = 1600$. For all the samples, we compute the target data, i.e. the field in dB, with the proposed parallel two-way SSW method. An example of a sample and the associated target is given in Fig. 4.

For the training procedure, this dataset is divided into two sets: the training set consisting of 80% of the samples and the test set consisting of the rest, i.e. 20%, of the samples. This partitioning is carried out for each subset associated with a specific number of obstacles, thereby preventing potential misrepresentation.

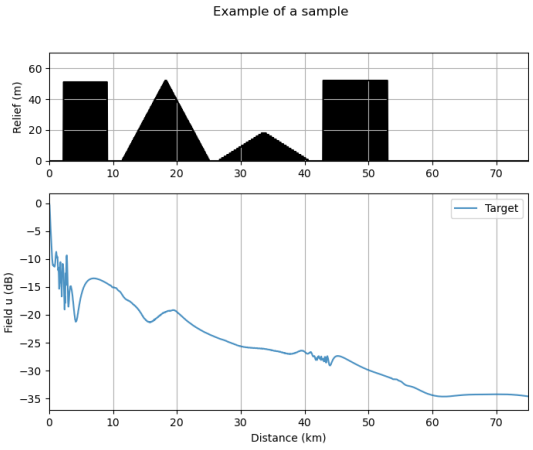

Fig. 4: Example of a sample for the dataset. The terrain and the corresponding field are plotted.

It should be noted that this sampling strategy can be easily generalized to introduce more obstacles or other physical phenomena, such as the terrain composition.

Finally, to solve the problem (4), we employ a usual Adam optimizer [19] for the stochastic gradient descent. In addition,

to mitigate overfitting, some dropout layers with a probability $p = 0.5$ are introduced in the descending stage. Furthermore, the bias of the last layer is set to the mean of the path loss across the training samples to accelerate the training process.

C. Some numerical results

1) Validation of the training procedure: In this part, the objective is to validate the training process of the network.

First, in Fig. 5, we show the convergence of the loss with the number of epochs of the optimization process.

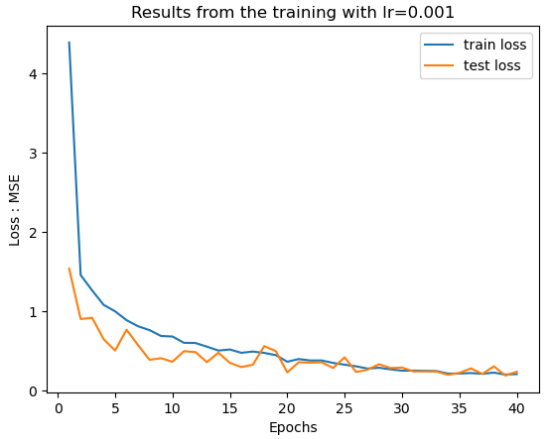

Fig. 5: Convergence of the loss over the training or test dataset with the number of epochs.

One can see that the training procedure decreases, and converges. Besides, the use of the mean of the field as the bias of the last layer allows us to begin with a lower loss. Finally, the better network, in terms of validation loss, is found at epoch 38 and kept from now on.

Second, the training is further validated by computing the path loss with the obtained network on a terrain with 6 obstacles. Indeed, this input is not in the training dataset. In Fig. 6, we plot the predicted field for a random sample of the terrain with 6 reliefs. The predicted fields with one-way and two-way SSW are also presented for comparison.

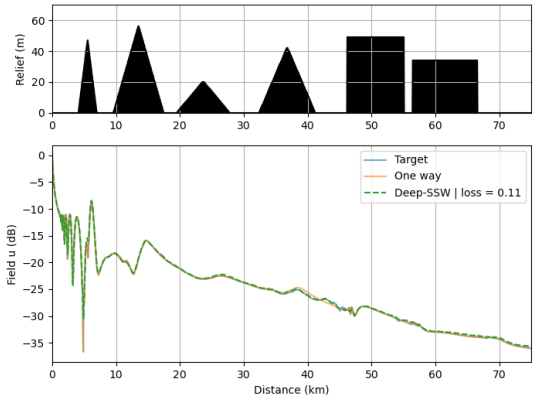

Fig. 6: Predicted path loss for an input terrain of 6 obstacles.

We can conclude that the training process has worked well. Indeed, the predicted field is very close to the one computed with two-way SSW (the target), as can be seen with the loss of 0.11, and mostly due to the highly oscillating part due to diffraction near the first obstacle. Besides, one can see that training with two-way SSW allows us to take into account the backward propagation since between 40 and 50 km the predicted field is close to the one computed with two-way SSW but differs from the one obtained with the one-way method.

2) Application: propagation from Paris to Chartres: In this section, the proposed Deep-twoway-SSW method is tested with true IGN [17] terrain data. The idea is to see how accurate the method is for real-life applications. Thus, we compare the machine-learning algorithm to two-way SSW. In this test, we compute the field from Paris to Chartres, two French cities distant by around 80 km and with a usual rural terrain elevation. Nonetheless, to be in between the altitude bounds of the LHS sampling, we normalize the IGN profile to 60 m at most. The terrain and the computed fields with two-way SSW and its Deep version are plotted in Fig. 7.

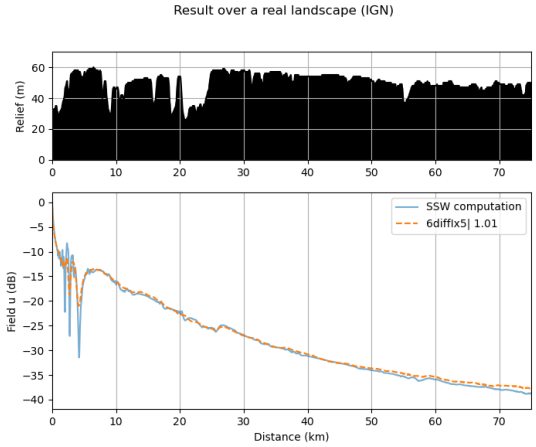

Fig. 7: Propagation from Paris to Chartres computed with both SSW and Deep-SSW.

As expected, since the data are completely different from the ones used to train Deep-twoway-SSW the MSE has increased but is still low. Nonetheless, the overall variation of the field has been well retrieved by the machine-learning method. The main errors come from the very low and rapidly oscillating extrema due to the diffraction from the rough part at the beginning of the domain.

Finally, the inference time here is below 0.07 s, almost in real-time on a conventional desktop computer. Therefore, Deep-twoway-SSW allows an accurate first glance at the propagation even with real landform data.

V. Conclusions and Perspectives

In this article, we derived a parallel version of the two-way SSW, addressing its computational problem. Indeed, the parallel method allows a drastic reduction in terms of computation time. In addition, we leverage this enhancement to train a machine-learning network to predict radar coverage in rural environments.

Numerical tests have been provided in the UHF band to highlight the advantages of the parallel two-way SSW method. In particular, we observe a gain of 25% to 60% depending on the terrain considered, while, as expected, the accuracy remains the same.

Furthermore, the derived Deep-twoway-SSW method has shown promising results using a modified U-Net architecture, together with a training dataset created in order to respect the underlying physical model.

In future works, we plan to hybridize the parallel two-way SSW method with the Method of Moments in order to model the effect of targets, such as wind turbines or ships, on the propagation. We also intend to further study the machine-learning network to optimize and generalize it for 2D inputs.

ACKNOWLEDGMENT

The authors wish to thank the DGA-AID (Direction Générale de l'Armement / Agence de l'Innovation de Défense, France) for its support of the MEPOM project, where this work is in progress.

REFERENCES

[1] J. R. Kuttler and G. D. Dockery, "Theoretical description of the parabolic approximation/fourier split-step method of representing electromagnetic propagation in the troposphere," *Radio Science*, vol. 26, no. 2, pp. 381–393, 1991.

[2] D. Dockery and J. R. Kuttler, "An improved impedance-boundary algorithm for Fourier split-step solutions of the parabolic wave equation," *IEEE Transactions on Antennas and Propagation*, vol. 44, no. 12, pp. 1592–1599, 1996.

[3] M. Levy, *Parabolic equation methods for electromagnetic wave propagation*. No. 45, IET, 2000.

[4] H. Zhou, A. Chabory, and R. Douvenot, "A fast wavelet-to-wavelet propagation method for the simulation of long-range propagation in low troposphere," *IEEE Transactions on Antennas and Propagation*, vol. 70, no. 3, pp. 2137–2148, 2021.

[5] T. Bonnafont, R. Douvenot, and A. Chabory, "A local split-step wavelet method for the long range propagation simulation in 2D," *Radio science*, vol. 56, no. 2, pp. 1–11, 2021.

[6] T. Bonnafont, R. Douvenot, and A. Chabory, "3d split-step wavelet method for the propagation over impedance ground condition," in *2021 XXXIVth General Assembly and Scientific Symposium of the International Union of Radio Science (URSI GASS)*, pp. 01–04, IEEE, 2021.

[7] O. Ozgun, "Recursive two-way parabolic equation approach for modeling terrain effects in tropospheric propagation," *IEEE Transactions on Antennas and Propagation*, vol. 57, no. 9, pp. 2706–2714, 2009.

[8] O. Ozgun, G. Apaydin, M. Kuzuoglu, and L. Sevgi, "PETOOL: MATLAB-based one-way and two-way split-step parabolic equation tool for radiowave propagation over variable terrain," *Computer Physics Communications*, vol. 182, no. 12, pp. 2638–2654, 2011.

[9] T. Bonnafont, O. Benhmammouch, and A. Khenchaf, "A two-way split-step wavelet scheme for tropospheric long-range propagation in various environments," *Remote Sensing*, vol. 14, no. 11, p. 2686, 2022.

[10] G. Y. Altun and O. Ozgun, "Electromagnetic propagation modeling over irregular terrain using a new hybrid method," in *2018 18th Mediterranean Microwave Symposium (MMS)*, pp. 258–261, IEEE, 2018.

[11] A. Seretis and C. D. Sarris, "An overview of machine learning techniques for radiowave propagation modeling," *IEEE Transactions on Antennas and Propagation*, vol. 70, no. 6, pp. 3970–3985, 2021.

[12] C. Brennan and K. McGuinness, "Site-specific deep learning path loss models based on the method of moments," in *2023 17th European Conference on Antennas and Propagation (EuCAP)*, pp. 1–5, IEEE, 2023.

[13] O. Ronneberger, P. Fischer, and T. Brox, "U-net: Convolutional networks for biomedical image segmentation," in *Medical Image Computing and Computer-Assisted Intervention–MICCAI 2015: 18th International Conference, Munich, Germany, October 5-9, 2015, Proceedings, Part III 18*, pp. 234–241, Springer, 2015.

[14] S. Bakirtzis, K. Qiu, J. Zhang, and I. Wassell, "DeepRay: Deep learning meets ray-tracing," in *2022 16th European Conference on Antennas and Propagation (EuCAP)*, pp. 1–5, IEEE, 2022.

[15] G. A. Deschamps, "Gaussian beam as a bundle of complex rays," *Electronics letters*, vol. 7, no. 23, pp. 684–685, 1971.

[16] T. Bonnafont, R. Douvenot, and A. Chabory, "Determination of the thresholds in split-step wavelet to assess accuracy for long-range propagation," *Radio Science Letters*, vol. 3, 2021.

[17] "Elevation lines data of the "Institut nationale de l'informations Géographique et Forestière" (IGN)." https://www.geoportail.gouv.fr/. Accessed: 03-05-2023.

[18] E. E. Gossard, G. EE, and S. RG, "Radar observation of clear air and clouds," 1983.

[19] D. P. Kingma and J. Ba, "Adam: A method for stochastic optimization," *arXiv preprint arXiv:1412.6980*, 2014.